2017

Defect Engineering: A Path toward Exceeding Perfection

Hamed Attariani
Wright State University - Lake Campus, hamed.attariani@wright.edu

Kasra Momeni

Kyle Adkins
Wright State University - Main Campus

ACS OMEGA

Article

http://pubs.acs.org/journal/acsodf

Defect Engineering: A Path toward Exceeding Perfection

Hamed Attariani,*[,†,‡] Kasra Momeni,[§] and Kyle Adkins[†]

[†]Department of Mechanical and Materials Engineering, Wright State University, Dayton, Ohio 45435, United States

[‡]Engineering Program, Wright State University - Lake Campus, Celina, Ohio 45822, United States

[§]Department of Mechanical Engineering, Louisiana Tech University, Ruston, Louisiana 71272, United States

Supporting Information

ABSTRACT: Moving to nanoscale is a path to get perfect materials with superior properties. Yet defects, such as stacking faults (SFs), are still forming during the synthesis of nanomaterials and, according to common notion, degrade the properties. Here, we demonstrate the possibility of engineering defects to, surprisingly, achieve mechanical properties beyond those of the corresponding perfect structures. We show that introducing SFs with high density increases the Young's Modulus and the critical stress under compressive loading of the nanowires above those of a perfect structure. The physics can be explained by the increase in intrinsic strain due to the presence of SFs and overlapping of the corresponding strain fields. We have used the molecular dynamics technique and considered ZnO as our model material due to its technological importance for a wide range of electromechanical applications. The results are consistent with recent experiments and propose a novel approach for the fabrication of stronger materials.

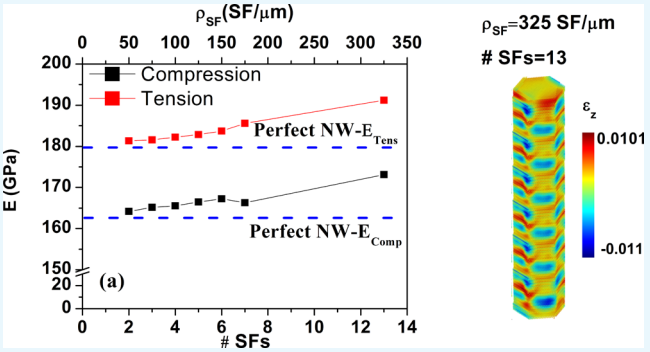

1. INTRODUCTION

Nanomaterials have a number of high-energy partially coordinated surface atoms that are comparable to the volume of their low-energy fully coordinated atoms. This forms the root of their size-dependent properties, such as enhancement of mechanical and piezoelectric properties by reducing the size.[1−4] This size dependence provides an additional controlling parameter for tailoring the characteristics of nanostructures. Defect engineering on the nanoscale is another fascinating possibility for building materials with various properties. Defects such as stacking fault (SF), twinning, vacancies, and interstitials are generally formed during the nanostructure fabrication process, which can modify the mechanical,[5−7] electrical,[8] and optical properties.[9,10] Among different types of nanostructures, one-dimensional nanostructures, for example, nanowires (NWs), nanotubes (NTs), and nanobelts (NBs), have been attracting significant attention from the research community due to their wide range of applications, such as composite reinforcement,[11,12] energy harvesting,[13,14] sensors,[15,16] light-emitting diodes,[17,18] and hybrid energy storage systems.[19,20] Therefore, tailoring and improving their properties, specifically, the mechanical properties, is key for their effective utilization.

The common understanding is that (points and planar) defects weaken the mechanical properties of nanostructures.[7,21−26] However, recent experiments on GaAs NWs depicted that introducing a high density of SFs increases the compressive critical stress and Young's Modulus.[5,6] In this case, interestingly, the Young's Modulus of defected NWs is even greater than that of the perfect wurtzite (WZ) structure. It is worth mentioning that despite the experimental evidence previous molecular dynamics simulations could not capture this phenomenon.[5]

Here, we explore the material design space using the two aforementioned additional design parameters, that is, defect concentration and size, and demonstrate tailoring the material properties by engineering their coupled effect. We have considered the ZnO NWs as the model material and have shown that planar defects can strengthen NWs beyond that of the ones with perfect structure. Our results indicate that the Young's Modulus of NWs, surprisingly, increases as the density of the SFs increases in the NWs. Also, although the critical stress increases by introducing more SFs for the compressive loading, it has an inverse effect on the critical stress for tensile loading. This unique behavior is explained by the localized longitudinal (c axis) stress and strain at defect sites. The interplay between SFs and free surfaces is the other cause of this effect. At the bulk, SFs are typically embedded between partial dislocations,[27] whereas at the nanoscale, they are confined between free surfaces. In the latter case, the SF creates a step at the surface, changing the local crystal structure,

Received: December 13, 2016
Accepted: February 10, 2017
Published: February 23, 2017

DOI: 10.1021/acsomega.6b00500
ACS Omega 2017, 2, 663−669

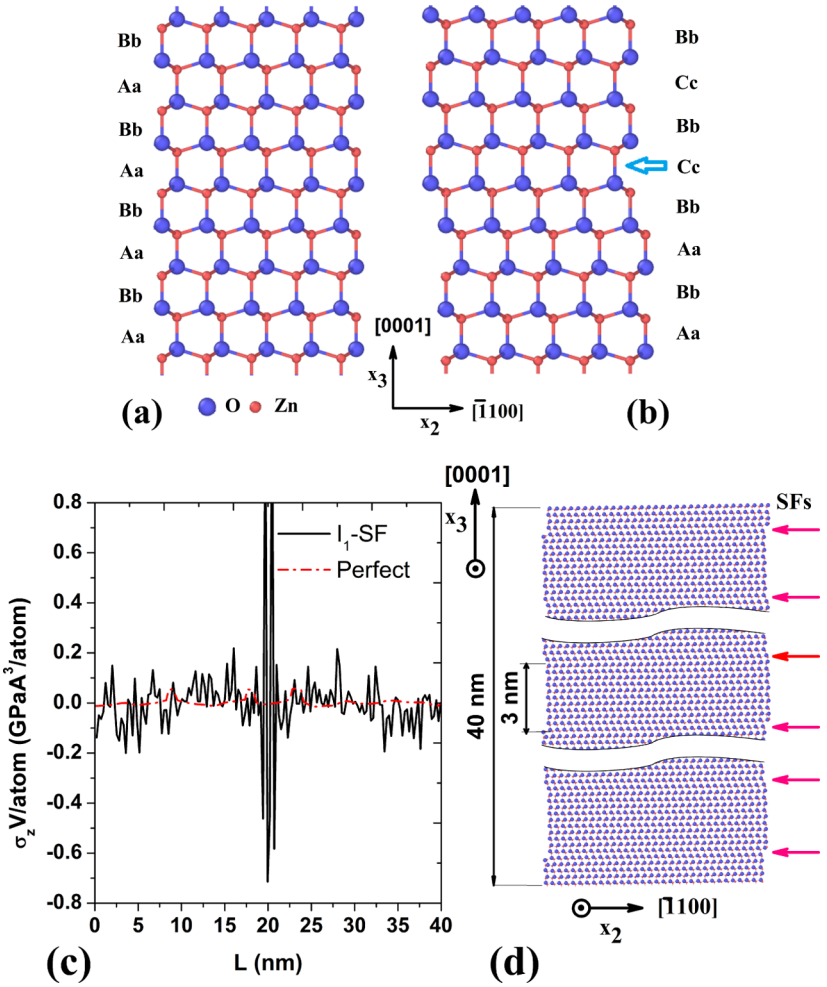

Figure 1. (a) Perfect WZ stacking sequence along the [0001] direction, where the uppercase and lowercase letters refer to O and Zn atoms in the same layer, respectively. (b) The stacking sequence for I_1-SF, where the arrows show the SF locations. (c) Longitudinal stress distribution along the *c* axis for a perfect NW (dotted line) and a NW with a single defect (solid line). (d) Structure of a WZ NW with 13 SFs within 40 nm length.

which may alter the overall electromechanical properties of the NWs.

2. NUMERICAL MODEL: DEVELOPMENT AND VALIDATION

SFs, one of the most common types of planar defects in II−VI and III−VI semiconductor nanostructures,[28−30] are categorized into two types: (i) basal-plane and (ii) prismatic-plane SFs. Here, we have developed a numerical model for the mechanics of I_1-SF in WZ ZnO, which has the lowest formation energy, 15 meV/unit-cell area,[31] among the different basal-plane SFs (I_1, I_2, E) of WZ. The I_1-SF Burger vector ($\vec{b}_{I1}$) in ZnO is (1/3) [01$\bar{1}$ 0] + (1/2) [0001],[28] which is generated by removing a layer of *c*-plane atoms and moving the rest by $\vec{b}_{I1}$. The perfect WZ structure has a stacking sequence of ...AaBbAaBbAaBbAaBbAa..., where the uppercase and lowercase letters refer to Zn and O atoms in two consecutive layers, respectively, whereas I_1-SF changes the stacking sequence to ...AaBbAaBbCcBbCcBbCc... (Figure 1a,b). Periodic boundary conditions are applied along the *c* axis, to mimic a long NW, and lateral directions are considered to be free. A Buckingham-type interatomic potential is utilized with Binks' fitted parameters for ZnO[32] (Table S1 in Supporting Information), which correctly captures its mechanical and surface properties and has been successfully used to study ZnO nanostructures. Also, the developed atomistic model is verified as it reproduces the reported experimental and numerical electromechanical properties of perfect ZnO NWs.[3,4,33−37]

Numerical simulations of the defected structure are performed by initially relaxing the NW for 100 ps at the simulation temperature, T = 0.01 K, under microcanonical ensemble (NVE). Then, the isothermal−isobaric ensemble (NPT) with a Nosé−Hoover thermostat is applied for another 100 ps to find the final relaxed configuration. In the last stage, a constant strain rate of ±0.001 fs^{-1} is applied along the *c* axis to model the mechanical response of the NW under tension/compression. Similar simulations are performed for a strain rate of ±0.0001 fs^{-1} to ensure that the results are independent of strain rate. The Young's Modulus is estimated by fitting a linear expression on the early section of the stress−strain curve, $\epsilon < 0.01$; this stands for the initial stage of loading. The numerical model is implemented in the large-scale atomic/molecular massively parallel simulator (LAMMPS) code,[38] and a time step of 1 fs is chosen for all simulation steps.

One of the classical problems in atomistic simulations of defects is the long-range interaction between the defects in a simulation cell and their corresponding periodic images. To overcome this issue and model a single SF, NWs of different

DOI: 10.1021/acsomega.6b00500
ACS Omega 2017, 2, 663−669

lengths are modeled and each relaxed longitudinal stress field was compared to that of the similar perfect NW. Our simulations indicate that the long-range interactions between a SF and its image in a periodic cell are negligible for NWs of length 40 nm and longer (Figure 1c). Here, to avoid ambiguities in calculating the stress using atomistic simulations due to unclear definition of the structure volume at such scales, we have used a representative stress, σ^* (= σ_z V/atom), to illustrate the effect of SF on stress distribution within the structure. High peaks appear at the defect, which rapidly decay toward the periodic boundaries (Figure 1c); that is, at the periodic boundaries, the stresses of the perfect and defective NWs is almost the same. Thus, a length of 40 nm is chosen for all simulated NWs here, whereas their diameters vary from 3 to 10 nm to study the effect of size. Furthermore, the effect of defect density on mechanical behavior is investigated by introducing numerous SFs, up to 13, in 40 nm length of a perfect NW. Therefore, the distance between two adjacent SFs varies from 20 to 3 nm for different defect densities. Figure 1d shows the schematic of a defected NW with 13 SFs in 40 nm length of the NW, which results in a distance of 3 nm between two adjacent SFs.

3. RESULTS AND DISCUSSION

By applying periodic boundary conditions in all directions, we have calculated the Young's Modulus of bulk ZnO to be 146 GPa, which is in close agreement with the reported experimental value, ≈140 GPa,[39−41] and verifies the developed model. Also, the formation energy of I_1-SF is calculated using the Binks potential to ensure its capability for predicting the properties of the faulted structure. The calculated I_1-SF energy is 14.1 meV/unit-cell area, which is in good agreement with density functional theory calculations, 15 meV/unit-cell area[31] (see Supporting Information for detailed calculations). The interaction between the defects and size scale on the structural properties of NWs is studied by introducing a single I_1-SF in the middle of 40 nm long ZnO NWs of various diameters and measuring their tension/compression response.

3.1. Mechanical Response and Size Dependence. The stress gradually increases to reach a maximum, called critical stress, where phase transformation occurs to release the accumulated elastic energy that results in the stress drop (see Figure S2). At the critical stress, the original WZ structure transforms into a graphite-like (HX) phase under compression and a body-centered tetragonal phase under tension.[4,34,36] However, in the presence of a SF, the NW breaks at the SF under tensile loading without any phase transition because the defect acts as an active site for crack initiation and the NW cannot store enough elastic energy to initiate the phase transition (Figure S2). In contrast, under compression, we still observed the WZ → HX phase transition.

Variations of the Young's Modulus and critical stress versus diameter for perfect and defective (with a single I_1-SF) NWs are plotted in Figure 2a. Although the variation of Young's Modulus in the presence of a single SF is negligible (Figure 2a), the critical stress generally reduces by introducing a SF (Figure 2b), and this effect is more pronounced for NWs with a diameter smaller than 4 nm. The difference in the strength (critical stresses) of defective and perfect NWs decreases by increasing their diameters.

The overall size dependence of Young's Modulus at a nanoscale was frequently reported, using both experimental[2,35] and theoretical approaches,[4,33,42,43] and was associated with the

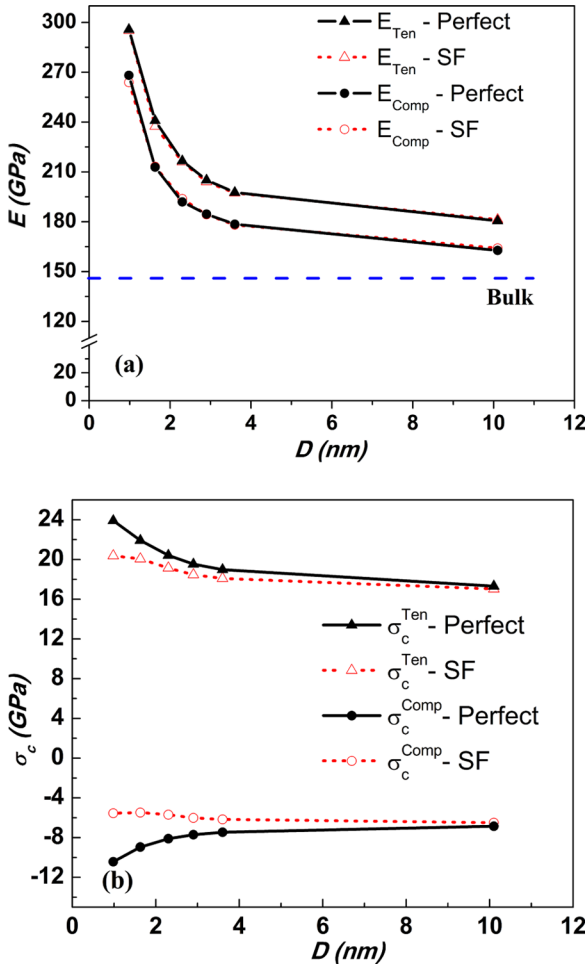

Figure 2. Effect of I_1-SF on the size-dependent mechanical response of ZnO NWs. (a) Young's Modulus of perfect and defective (single SF) NWs under compression/tension vs diameter, which show negligible effect of SF. (b) Variation of critical stress σ_c as a function of diameter under compression/tension, which indicates larger reduction of σ_c for thinner NWs as SF is introduced into their structure. The superscripts Ten and Comp stand for tensile and compression test, respectively.

surface stress contribution. One well-known explanation is based on the core−shell model,[44] where a shell (outer layers) is under compressive stress due to surface stresses and the core (inner layers) is under tension. The compressive stress at the shell causes surface stiffening and increases the overall Young's Modulus of the NWs with smaller diameters. The gap between critical stresses of defective and perfect NWs can be explained by the intrinsic strain distribution along the longitudinal direction, [0001], of the relaxed structure. The longitudinal strain, ϵ_z, is calculated using OVITO[45−47] and is shown in Figure 3. The SF induces intrinsic tensile strain at defect sites and compressive strain at the defect surrounding, which causes reduction in the critical stress. The size dependence of the difference between the critical stresses of defective and perfect NWs can be justified by the interplay between the surface and SF energies. Generally, reducing the system size leads to an increase in the total energy density because of the increase in the surface energy. Therefore, introducing SFs into a NW of smaller diameter requires more energy per atom in comparison to that for a larger-diameter NW, which is the source for the size dependence of the critical stress difference between perfect and defective NWs. This has also been verified experimentally

DOI: 10.1021/acsomega.6b00500
ACS Omega 2017, 2, 663−669

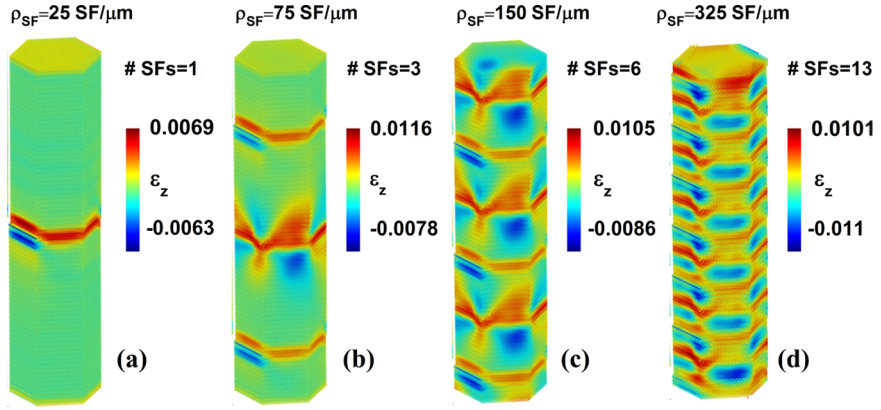

Figure 3. Longitudinal strain, ϵ_z, for NWs with different defect densities and a diameter of 10 nm. Results for (a) 1 SF, (b) 3 SFs, (c) 6 SFs, and (d) 13 SFs are presented, which indicate complexity and interference of strain field as the number of SFs increases.

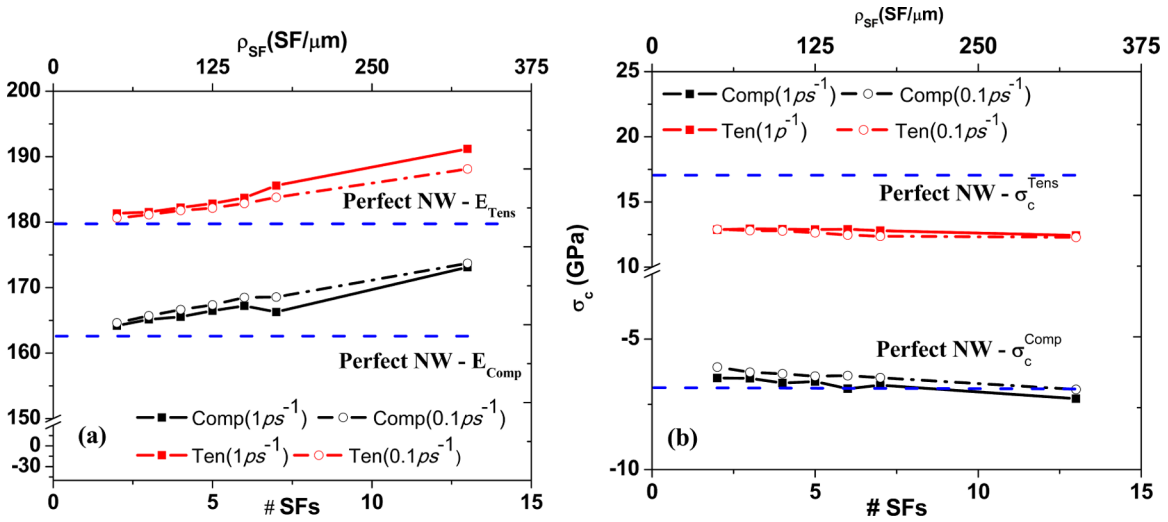

Figure 4. Effect of SF density on the mechanical response of NWs. (a) Variation of tensile/compressive Young's Modulus vs density of SFs, indicating that a higher Young's Modulus can be obtained by introducing higher defect densities in the NW. (b) Effect of SF density on the critical stress, revealing degradation of this material property for the tensile loading, whereas it shows slight improvement under compressive loading and small defect densities. All simulated NWs have the same diameter of 10 nm. The properties of a perfect NW are shown with dotted lines.

for III−V NWs,[48] for which the SF density depletes with decreasing diameter and a perfect WZ NW can be produced by reducing its diameter.

3.2. Defect Density. The possibility of tailoring the mechanical properties of nanostructures through defect engineering was investigated by introducing multiple SFs with a constant separation distance into a ZnO NW of 10 nm diameter. The spacing between SFs ranges from 3 to 20 nm for different defect densities, that is, number of SFs in unit length (ρ_{SF}). Variations of the Young's Modulus and critical stress as a function of the number of defects within 40 nm length (i.e., defect density, ρ_{SF}) are plotted in Figure 4 for both tensile and compressive loadings. Our results show that increasing the ρ_{SF} gradually increases the Young's Modulus in tension and compression. However, no drastic changes in the critical stress were captured in tension and only a slight increase was observed for compressive loading. Our simulations show that introducing a high density of SFs, SF = 13, into a perfect structure leads to a 6.23% increase in critical stress (the critical stresses are summarized in Table S2). Surprisingly, the Young's Modulus of a highly defective NW (13 SFs in a 40 nm long NW) is even higher than that of the perfect NWs, a result that is nontrivial. This finding opens up a novel approach for synthesizing nanostructures with a higher Young's Modulus through defect engineering. The stress−strain curves are depicted in Figure S3 for more reference. It is worth mentioning that this behavior was observed experimentally for GaAs NWs under buckling; however, they could not capture this physics using atomistic simulations.[5,6] The effect of strain rate on the mechanical properties of NWs is a well-known phenomenon.[49] Therefore, all simulations were repeated by lowering the strain rate by 1 order of magnitude, 0.0001 fs^{-1}, to investigate the impact of this parameter on the ascending trend of Young's Modulus. Our results (Figure 4) show that despite the lower strain rate Young's Modulus still increases by increasing the number of SFs.

The underlying physics is multifaceted, which may lie in changes of the bond nature around defects, as proposed in refs 5 and 6. The effect of SF on the atomistic structure of WZ NW is shown in Figure 5, which reveals the formation of a step at the defect site after relaxation. At the intersection of SF and free surface, surface stresses cause a severe local deformation. At the intersection of SF and the $[01\bar{1}\,0]$ surface, the bond length of Zn−O, located at the inner layer, represented by b_1, decreases from 1.978 Å in a perfect crystal to 1.884 Å in the deformed structure. The out-of-plane Zn−O bond length, denoted b_2, is

DOI: 10.1021/acsomega.6b00500
ACS Omega 2017, 2, 663−669

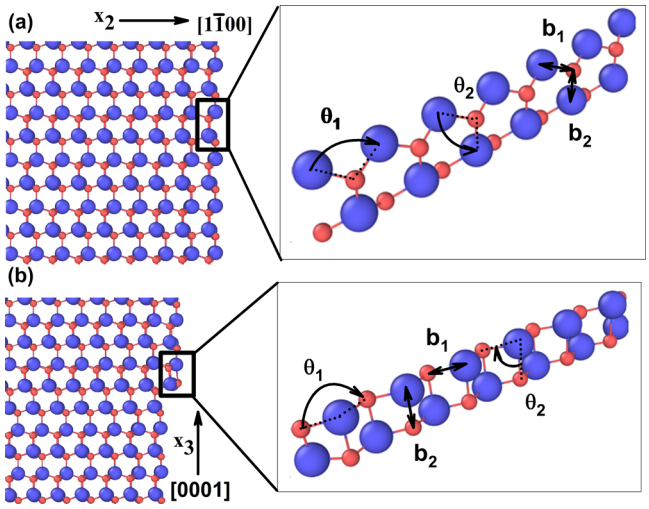

Figure 5. Effect of SF on the atomic structure of a ZnO NW. (a) Perfect WZ crystal structure in the absence of SF on the [01$\bar{1}$0] surface. (b) The crystal structure at the intersection of SF and the [01$\bar{1}$0] surface.

2.141 Å, whereas the out-of-plane bond length in the perfect structure is 2.005 Å. Also, the in-plane bond angle, θ_1, is 123.112° in the highly deformed zone, whereas this value decreases to 120.303° for a perfect WZ. Finally, the out-of-plane angle, θ_2, is 91.871° for the defective (single I_1-SF) and 111.458° for a perfect structure. These variations in the bond length/angle can be used to verify the change in mechanical properties of the nanostructure, that is, $E \propto d^{-4}$, where d and E are the bond length and Young's Modulus, respectively.[50] Introducing more SFs results in a larger change in the bond length and angle, which consequently alters the mechanical response of the system. Another explanation for this phenomenon can be given by considering the strain distribution in the relaxed structure. The intrinsic longitudinal strain in the presence of multiple SFs is depicted in Figure 3b–d for different defect densities and indicates that the tensile strain is induced at SF sites, whereas compressive strain appears at the upper and lower regions of the SFs. As the density of SFs increases, the tensile strain slightly decreases from 0.0116 to 0.0101, whereas the compressive strain increases from −0.0078 to −0.011. This change in the longitudinal strain is due to the overlap between the strain fields of adjacent SFs. Referring to the core–shell model, increasing the compressive strain at the shell leads to a reduction in bond length and a higher Young's Modulus for the NWs.

To explore the effect of SF density on the critical stress, the similar reasoning can be used. The sharp stress drop in the stress–strain curve of ZnO NWs (Figures S2 and S3) can be explained by the phase transition in ZnO NWs. During loading, the NW stores energy in the form of elastic energy until a critical value is reached. At this point, the stored energy will be released by the phase transition mechanism. In compression, a new HX phase nucleates from the surface and at some distance from the SF (see Figure S2). This can be described by the formation of highly localized deformed regions around SFs, which change the bond type and crystal structure (Figure 5). These domains are not the ideal sites for nucleation; hence, the nucleation site will be shifted away from the SF locations. Increasing the number of SFs increases the number of these deformed zones and consequently limits the possibility of HX phase nucleation. This leads to an increase in the energy required for activating the phase transition mechanism and subsequently an increase in the compressive critical stress.

4. CONCLUSIONS

In summary, we have investigated the possibility of applying defect engineering to tailor the mechanical response of nanostructures, using an atomistic modeling approach with ZnO NWs as our model material. The simulations revealed that introducing a higher density of I_1-SFs will increase the Young's Modulus beyond that of the corresponding perfect structure under both tensile and compressive loadings. Also, a highly defective NW exhibits a higher strength under compression test, whereas SFs reduce the tensile strength. The reason behind this higher Young's Modulus can be the change in the bond length and overlapping of the SF strain fields. To study the changes in the bond types and lengths, a detailed study using ab initio techniques is required. Additionally, the interaction between the surface energy and the SF intrinsic stress predicts that adding the SFs in smaller NWs can have a drastic impact on the mechanical properties of a material. The results presented here suggest new routes for fabrication of NWs with superior mechanical properties.

Considering the fact that intrinsic strain can mediate the properties of nanostructures, additional detailed studies are required to explore the effect of SFs on the electrical, optical, and electromechanical response of NWs.[51,52] Also, there is a feasibility to increase the NW activity by introducing SFs as active sites for chemical reactions; thus, chemical activity of a material can be tailored by introducing a proper distribution of SFs. Furthermore, studying the effects of other types of SFs, I_2 and E, point defects, and twin boundary on material response would be another promising avenue for exploration.[53,54] Finally, the possibility of strengthening a nanostructure via synthesizing the WZ/zinc blende (ZB) polytype structures can be examined, that is, the SFs are observed at the WZ/ZB interface.

■ ASSOCIATED CONTENT

Supporting Information

The Supporting Information is available free of charge on the ACS Publications website at DOI: 10.1021/acsomega.6b00500.

Strain–stress curves for NWs and their corresponding phase transition in the presence of SFs and also the Buckingham potential parameters and calculation of SF formation energy (PDF)

■ AUTHOR INFORMATION

Corresponding Author

*E-mail: hamed.attariani@wright.edu.

ORCID

Hamed Attariani: 0000-0002-4777-5116

Author Contributions

H.A. and K.M. performed the analysis and prepared the manuscript. K.A. performed the molecular dynamic simulations.

Notes

The authors declare no competing financial interest.

■ ACKNOWLEDGMENTS

The support of Wright State University and Louisiana Tech University are gratefully acknowledged. This project is also partly supported by Louisiana EPSCoR-OIA-1541079

DOI: 10.1021/acsomega.6b00500
ACS Omega 2017, 2, 663–669

(NSF(2017)-CIMMSeed-10). The authors would like to thank Ohio Super Computing (OSC), Grant No. ECS- PWSU0463, and Louisiana Optical Network Initiative (LONI) for providing the computational resources. Also, we thank Drs. A. Soghrati and B. Shiari for supporting this research in part through computational resources by National Nanotechnology Infrastructure Network Computation (NNIN/C) project at University of Michigan, which is supported by the National Science Foundation under Grant No. ECS-0335765.

REFERENCES

(1) Fan, H. J.; Lee, W.; Hauschild, R.; Alexe, M.; Le Rhun, G.; Scholz, R.; Dadgar, A.; Nielsch, K.; Kalt, H.; Krost, A.; et al. Template-Assisted Large-Scale Ordered Arrays of ZnO Pillars for Optical and Piezoelectric Applications. *Small* **2006**, *2*, 561−568.

(2) Asthana, A.; Momeni, K.; Prasad, A.; Yap, Y.; Yassar, R. In situ observation of size-scale effects on the mechanical properties of ZnO nanowires. *Nanotechnology* **2011**, *22*, No. 265712.

(3) Agrawal, R.; Espinosa, H. D. Giant piezoelectric size effects in zinc oxide and gallium nitride nanowires. A first principles investigation. *Nano Lett.* **2011**, *11*, 786−790.

(4) Momeni, K.; Attariani, H. Electromechanical properties of 1D ZnO nanostructures: nanopiezotronics building blocks, surface and size-scale effects. *Phys. Chem. Chem. Phys.* **2014**, *16*, 4522−4527.

(5) Chen, B.; Wang, J.; Gao, Q.; Chen, Y.; Liao, X.; Lu, C.; Tan, H. H.; Mai, Y.-W.; Zou, J.; Ringer, S. P.; et al. Strengthening brittle semiconductor nanowires through stacking faults: insights from in situ mechanical testing. *Nano Lett.* **2013**, *13*, 4369−4373.

(6) Chen, Y.; Burgess, T.; An, X.; Mai, Y.-W.; Tan, H. H.; Zou, J.; Ringer, S. P.; Jagadish, C.; Liao, X. Effect of a High Density of Stacking Faults on the Young's Modulus of GaAs Nanowires. *Nano Lett.* **2016**, *16*, 1911−1916.

(7) Lucas, M.; Wang, Z. L.; Riedo, E. Combined polarized Raman and atomic force microscopy: In situ study of point defects and mechanical properties in individual ZnO nanobelts. *Appl. Phys. Lett.* **2009**, *95*, No. 051904.

(8) Schmidt-Mende, L.; MacManus-Driscoll, J. L. ZnO-nanostructures, defects, and devices. *Mater. Today* **2007**, *10*, 40−48.

(9) Heiss, M.; Conesa-Boj, S.; Ren, J.; Tseng, H.-H.; Gali, A.; Rudolph, A.; Uccelli, E.; Peiró, F.; Morante, J. R.; Schuh, D.; et al. Direct correlation of crystal structure and optical properties in wurtzite/zinc-blende GaAs nanowire heterostructures. *Phys. Rev. B* **2011**, *83*, No. 045303.

(10) Sieber, B.; Addad, A.; Szunerits, S.; Boukherroub, R. Stacking faults-induced quenching of the UV luminescence in ZnO. *J. Phys. Chem. Lett.* **2010**, *1*, 3033−3038.

(11) Malakooti, M. H.; Patterson, B. A.; Hwang, H.-S.; Sodano, H. A. ZnO nanowire interfaces for high strength multifunctional composites with embedded energy harvesting. *Energy Environ. Sci.* **2016**, *9*, 634−643.

(12) Kong, K.; Deka, B. K.; Kwak, S. K.; Oh, A.; Kim, H.; Park, Y.-B.; Park, H. W. Processing and mechanical characterization of ZnO/polyester woven carbon-fiber composites with different ZnO concentrations. *Composites, Part A* **2013**, *55*, 152−160.

(13) Kumar, B.; Kim, S.-W. Energy harvesting based on semiconducting piezoelectric ZnO nanostructures. *Nano Energy* **2012**, *1*, 342−355.

(14) Kim, K.-H.; Kumar, B.; Lee, K. Y.; Park, H.-K.; Lee, J.-H.; Lee, H. H.; Jun, H.; Lee, D.; Kim, S.-W. Piezoelectric two-dimensional nanosheets/anionic layer heterojunction for efficient direct current power generation. *Sci. Rep.* **2013**, *3*, No. 2017.

(15) Wang, H.-T.; Kang, B.; Ren, F.; Tien, L.; Sadik, P.; Norton, D.; Pearton, S.; Lin, J. Hydrogen-selective sensing at room temperature with ZnO nanorods. *Appl. Phys. Lett.* **2005**, *86*, No. 243503.

(16) Alenezi, M. R.; Henley, S. J.; Emerson, N. G.; Silva, S. R. P. From 1D and 2D ZnO nanostructures to 3D hierarchical structures with enhanced gas sensing properties. *Nanoscale* **2014**, *6*, 235−247.

(17) Bao, J.; Zimmler, M. A.; Capasso, F.; Wang, X.; Ren, Z. Broadband ZnO single-nanowire light-emitting diode. *Nano Lett.* **2006**, *6*, 1719−1722.

(18) Son, D. I.; Kwon, B. W.; Park, D. H.; Seo, W.-S.; Yi, Y.; Angadi, B.; Lee, C.-L.; Choi, W. K. Emissive ZnO-graphene quantum dots for white-light-emitting diodes. *Nat. Nanotechnol.* **2012**, *7*, 465−471.

(19) Reddy, A. L. M.; Gowda, S. R.; Shaijumon, M. M.; Ajayan, P. M. Hybrid nanostructures for energy storage applications. *Adv. Mater.* **2012**, *24*, 5045−5064.

(20) Yang, P.; Xiao, X.; Li, Y.; Ding, Y.; Qiang, P.; Tan, X.; Mai, W.; Lin, Z.; Wu, W.; Li, T.; et al. Hydrogenated ZnO core-shell nanocables for flexible supercapacitors and self-powered systems. *ACS Nano* **2013**, *7*, 2617−2626.

(21) Ghosh, M.; Ghosh, S.; Attariani, H.; Momeni, K.; Seibt, M.; Mohan Rao, G. Atomic defects influenced mechanics of II−VI nanocrystals. *Nano Lett.* **2016**, *16*, 5969.

(22) Lucas, M.; Mai, W.; Yang, R.; Wang, Z. L.; Riedo, E. Aspect ratio dependence of the elastic properties of ZnO nanobelts. *Nano Lett.* **2007**, *7*, 1314−1317.

(23) Yan, X.; Dickinson, M.; Schirer, J. P.; Zou, C.; Gao, W. Face dependence of mechanical properties of a single ZnO nano/microrod. *J. Appl. Phys.* **2010**, *108*, No. 056101.

(24) He, M.-R.; Zhu, J. Defect-dominated diameter dependence of fracture strength in single-crystalline ZnO nanowires: In situ experiments. *Phys. Rev. B* **2011**, *83*, No. 161302.

(25) Wang, X.; Chen, K.; Zhang, Y.; Wan, J.; Warren, O. L.; Oh, J.; Li, J.; Ma, E.; Shan, Z. Growth Conditions Control the Elastic and Electrical Properties of ZnO Nanowires. *Nano Letters* **2015**, *15*, 7886−7892.

(26) Liu, K.; Wang, W.; Xu, Z.; Liao, L.; Bai, X.; Wang, E. In situ probing mechanical properties of individual tungsten oxide nanowires directly grown on tungsten tips inside transmission electron microscope. *Appl. Phys. Lett.* **2006**, *89*, No. 221908.

(27) Suzuki, K.; Ichihara, M.; Takeuchi, S. High-resolution electron microscopy of extended defects in wurtzite crystals. *Jpn. J. Appl. Phys.* **1994**, *33*, No. 1114.

(28) Ding, Y.; Wang, Z. L. Structures of planar defects in ZnO nanobelts and nanowires. *Micron* **2009**, *40*, 335−342.

(29) Zardo, I.; Conesa-Boj, S.; Peiro, F.; Morante, J.; Arbiol, J.; Uccelli, E.; Abstreiter, G.; Morral, A. F. Raman spectroscopy of wurtzite and zinc-blende GaAs nanowires: polarization dependence, selection rules, and strain effects. *Phys. Rev. B* **2009**, *80*, No. 245324.

(30) Panda, J. K.; Roy, A.; Singha, A.; Gemmi, M.; Ercolani, D.; Pellegrini, V.; Sorba, L. Raman sensitivity to crystal structure in InAs nanowires. *Appl. Phys. Lett.* **2012**, *100*, No. 143101.

(31) Yan, Y.; Dalpian, G.; Al-Jassim, M.; Wei, S.-H. Energetics and electronic structure of stacking faults in ZnO. *Phys. Rev. B* **2004**, *70*, No. 193206.

(32) Binks, D. J.; Grimes, R. W. The non-stoichiometry of zinc and chromium excess zinc chromite. *Solid State Commun.* **1994**, *89*, 921−924.

(33) Dai, L.; Cheong, W.; Sow, C.; Lim, C.; Tan, V. Molecular dynamics simulation of ZnO nanowires: size effects, defects, and super ductility. *Langmuir* **2010**, *26*, 1165−1171.

(34) Wang, J.; Kulkarni, A.; Sarasamak, K.; Limpijumnong, S.; Ke, F.; Zhou, M. Molecular dynamics and density functional studies of a body-centered-tetragonal polymorph of ZnO. *Phys. Rev. B* **2007**, *76*, No. 172103.

(35) Agrawal, R.; Peng, B.; Gdoutos, E. E.; Espinosa, H. D. Elasticity size effects in ZnO nanowires- a combined experimental-computational approach. *Nano Lett.* **2008**, *8*, 3668−3674.

(36) Kulkarni, A. J.; Zhou, M.; Sarasamak, K.; Limpijumnong, S. Novel phase transformation in ZnO nanowires under tensile loading. *Phys. Rev. Lett.* **2006**, *97*, No. 105502.

(37) Momeni, K.; Attariani, H.; LeSar, R. A. Structural transformation in monolayer materials: A 2D to 1D transformation. *Phys. Chem. Chem. Phys.* **2016**, 19873−19879.

(38) Plimpton, S. Fast parallel algorithms for short-range molecular dynamics. *J. Comput. Phys.* **1995**, *117*, 1−19.

DOI: 10.1021/acsomega.6b00500
ACS Omega 2017, 2, 663−669

(39) Simmons, G.; Wang, H. *Single Crystal Elastic Constants and Calculated Aggregate Properties*; M.I.T. Press, 1971.
(40) Kobiakov, I. Elastic, piezoelectric and dielectric properties of ZnO and CdS single crystals in a wide range of temperatures. *Solid State Commun.* **1980**, *35*, 305−310.
(41) Bateman, T. Elastic moduli of single-crystal zinc oxide. *J. Appl. Phys.* **1962**, *33*, 3309−3312.
(42) Wang, J.; Kulkarni, A.; Ke, F.; Bai, Y.; Zhou, M. Novel mechanical behavior of ZnO nanorods. *Comput. Methods Appl. Mech. Eng.* **2008**, *197*, 3182−3189.
(43) Wang, J.; Xiao, P.; Zhou, M.; Wang, Z.; Ke, F. Wurtzite-to-tetragonal structure phase transformation and size effect in ZnO nanorods. *J. Appl. Phys.* **2010**, *107*, No. 023512.
(44) Chen, C.; Shi, Y.; Zhang, Y.; Zhu, J.; Yan, Y. Size dependence of Young's Modulus in ZnO nanowires. *Phys. Rev. Lett.* **2006**, *96*, No. 075505.
(45) Stukowski, A. Visualization and analysis of atomistic simulation data with OVITO-the Open Visualization Tool. *Modell. Simul. Mater. Sci. Eng.* **2009**, *18*, No. 015012.
(46) Shimizu, F.; Ogata, S.; Li, J. Theory of shear banding in metallic glasses and molecular dynamics calculations. *Mater. Trans.* **2007**, *48*, 2923−2927.
(47) Falk, M.; Langer, J. Dynamics of viscoplastic deformation in amorphous solids. *Phys. Rev. E* **1998**, *57*, No. 7192.
(48) Caroff, P.; Dick, K. A.; Johansson, J.; Messing, M. E.; Deppert, K.; Samuelson, L. Controlled polytypic and twin-plane superlattices in III−V nanowires. *Nat. Nanotechnol.* **2009**, *4*, 50−55.
(49) Setoodeh, A.; Attariani, H.; Khosrownejad, M. Nickel nanowires under uniaxial loads: A molecular dynamics simulation study. *Comput. Mater. Sci.* **2008**, *44*, 378−384.
(50) Harrison, W. A. *Electronic Structure and the Properties of Solids: the Physics of the Chemical Bond*; Dover Publications, 2012.
(51) Asthana, A.; Momeni, K.; Prasad, A.; Yap, Y.; Yassar, R. On the correlation of crystal defects and band gap properties of ZnO nanobelts. *Appl. Phys. A* **2011**, *105*, 909−914.
(52) Lähnemann, J.; Jahn, U.; Brandt, O.; Flissikowski, T.; Dogan, P.; Grahn, H. T. Luminescence associated with stacking faults in GaN. *J. Phys. D: Appl. Phys.* **2014**, *47*, No. 423001.
(53) Panda, J. K.; Roy, A.; Chakraborty, A.; Dasgupta, I.; Hasanu, E.; Ercolani, D.; Sorba, L.; Gemmi, M. Strain-induced band alignment in wurtzite/zinc-blende InAs heterostructured nanowires. *Phys. Rev. B* **2015**, *92*, No. 205302.
(54) Cheng, G.; Chang, T.-H.; Qin, Q.; Huang, H.; Zhu, Y. Mechanical properties of silicon carbide nanowires: effect of size-dependent defect density. *Nano Lett.* **2014**, *14*, 754−758.

DOI: 10.1021/acsomega.6b00500
ACS Omega 2017, 2, 663−669